AGU ADVANCING EARTH AND SPACE SCIENCES

Geophysical Research Letters®

RESEARCH LETTER
10.1029/2023GL105810

Key Points:

- Settling velocity of suspended sediments is reduced by virtual mass and Basset history for grains larger than turbulent micro-scales
- An operational Rouse-like budget that models these two effects is derived and tested against experiments
- Turbulent Schmidt number exceeding unity in the experiments can be linked to these two effects

Supporting Information:

Supporting Information may be found in the online version of this article.

Correspondence to:

S. Li,
sl3259@cornell.edu

Citation:

Li, S., Bragg, A. D., & Katul, G. (2023). Reduced sediment settling in turbulent flows due to Basset history and virtual mass effects. *Geophysical Research Letters*, *50*, e2023GL105810. https://doi.org/10.1029/2023GL105810

Received 7 AUG 2023
Accepted 14 OCT 2023

Reduced Sediment Settling in Turbulent Flows Due To Basset History and Virtual Mass Effects

Shuolin Li[1], Andrew D. Bragg[1], and Gabriel Katul[1]

[1]Department of Civil and Environmental Engineering, Duke University, Durham, NC, USA

Abstract The behavior of suspended particles in turbulent flows is a recalcitrant problem spanning wide-ranging fields including geomorphology, hydrology, and dispersion of particulate matter in the atmosphere. One key mechanism underlying particle suspension is the difference between particle settling velocity (w_s) in turbulence and its still water counterpart (w_{so}). This difference is explored here for a range of particle-to-fluid densities (1–10) and particle diameter to Kolmogorov micro-eddy sizes (0.1–10). Conventional models of particle fluxes that equate w_s to w_{so} result in eddy diffusivities and turbulent Schmidt numbers contradictory to laboratory experiments. Incorporating virtual mass and Basset history forces resolves these inconsistencies, providing clarity as to why w_s/w_{so} is sub-unity for the aforementioned conditions. The proposed formulation can be imminently used to model particle settling in turbulence, especially when sediment distribution outcomes over extended time scales far surpassing turbulence time scales are sought.

Plain Language Summary In rivers and streams, mixed-up dirt called "suspended sediments" is known to influence water quality and its concomitant effects on many physical, chemical, and biological processes. Suspended sediments can be harmful to aquatic ecosystem productivity because they reduce light penetration. They can clog gills of fish and other aquatic organism, and they can impact reservoir operation and their capacity necessitating frequent dredging. There is debate about how these sediments interact with swirling motions ("turbulent flows") in moving water. Traditional mathematical models overlook how individual grains are affected by these swirls ("turbulent eddies") and how they displace water ("virtual mass") when sediments move in a fluid. For large grains, these overlooked details can generate new terms in the force balance that are associated with complex eddying motion lagging behind the grain motion ("Basset history term"). Including the Basset history and virtual mass factors reconciles controversies between recent laboratory experiments and traditional theories about how grains settle in turbulent flows.

1. Introduction

The transport of sediments unquestionably influences many geomorphic processes manifesting themselves through erosion and deposition and delineation of river morphology. Describing sediment transport from turbulent time scales of fractions of seconds to geomorphic time scales of multiple years or even decades thus presents a significant research challenge but remains fundamental to numerous geophysical, ecological, and climate-related problems (Alonso-González et al., 2010; Davarpanah Jazi & Wells, 2016; Dey, 2014; Duman et al., 2016; Huang et al., 2020; J. Li & Osada, 2007; Scollo et al., 2005; Huai et al., 2021). In response, models that parameterize the interactive effects between turbulent flows and sediments are still being developed despite some 90 years of research (Rouse, 1937; Vanoni, 1984; Dey, 2014; von Kármán, 1934). Modeling the amount of sediment transported as suspended load in turbulent flows requires determining the turbulent sediment settling velocity w_s, which was conventionally approximated by the sediment settling velocity in still water w_{so} (Dey, 2014; Rouse, 1937; Shu & Fei, 2008; von Kármán, 1934). However, several settling velocity relations suggest that the particle physics related to large grain size in turbulent flows may not be adequately represented in such models (Dietrich, 1982; Ferry & Balachandar, 2001; Van Rijn, 1993; Wu & Wang, 2006). More recently, some studies have shown that turbulence can either enhance or reduce w_s compared to w_{so} (Good et al., 2014; Squires & Eaton, 1991) depending on several factors such as the relative grain size d_p/η (d_p is the grain diameter and η is the Kolmogorov microscale eddy size), relative density $s = \rho/\rho_p$ (ρ_p is grain density, ρ is fluid density), the Rouse number (R_*) and the Taylor micro-scale Reynolds number (Mora et al., 2021), among others. Four mechanisms have been proposed to broadly explain why $w_s/w_{so} \neq 1$ when grain-grain interactions are ignored in a dilute mixture (Akutina et al., 2020): (a) preferential sweeping, which yields $w_s/w_{so} > 1$ (Bragg et al., 2021; J. Li & Osada, 2007; Maxey, 1987; Tom & Bragg, 2019; Tom et al., 2022; Yang & Shy, 2005; Wang & Maxey, 1993), (b)

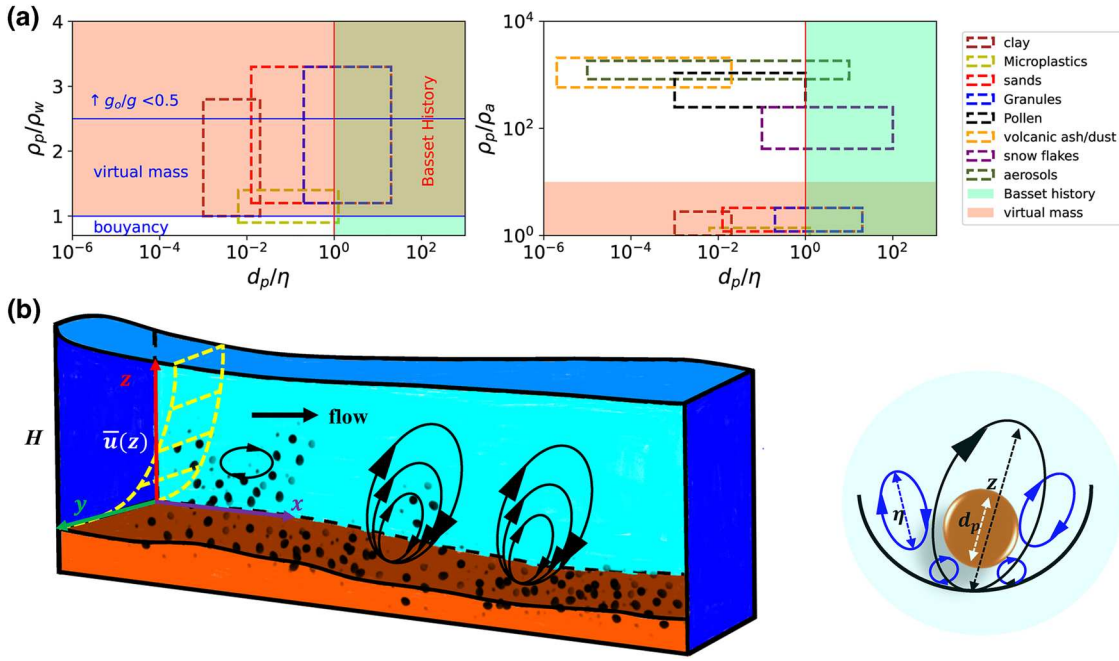

Figure 1. Top: Geophysical applications of particle settling in water (left) and air (right) organized by d_p/η and relative densities ρ_p/ρ, with $\rho = \rho_w$ for water and $\rho = \rho_a$ for air. The shaded regions indicate when the virtual mass (orange-red shaded) and Basset history (green shaded) terms can be significant. The applications include suspended sediment transport in rivers and conveyance structures, snow, aerosols, dust and ashes, and certain types of aggregate plastics in the atmosphere. Bottom: A sketch of an open channel flow with suspended sediments entrained from the channel bed (left) and a single grain (right) interacts with the micro-scale eddy (η) commensurate with d_p. The inclusion of virtual mass and Basset history terms in the mean sediment concentration budget become necessary when $d_p/\eta > 0.1$ and ρ_p/ρ is of order unity.

vortex trapping, (c) non-linear drag, and (d) loitering. The latter three mechanisms all result in $w_s/w_{so} < 1$ whereas the first leads to $w_s/w_{so} > 1$ (Fornari et al., 2016; Good et al., 2014). Preferential sweeping appears to dominate for $d_p/\eta \leq 1$ but for heavy inertial particles ($s \ll 1$) that tend to be swept into downdraft regions characterized by low vorticity and high stain rate (Squires & Eaton, 1991; Stout et al., 1995). Vortex trapping also occurs for small particles ($d_p/\eta \leq 1$) but for $R_* \ll 1$. When the difference between fluid and sediment velocity (or slippage velocity) fluctuates in time, a non-linear drag favors higher drag values over lower drag values resulting in a net increase in the effective drag coefficient sensed by the settling grain. Thus, averaging over the settling time yields a larger drag force resulting in $w_s/w_{so} < 1$ (Stout et al., 1995). Loitering can occur when sediments with finite inertia spend more time moving upward (which is assumed to take longer) than moving downward (which is assumed to take less time), resulting in an asymmetric behavior (Akutina et al., 2020). This behavior, partly connected to ejections dominating over sweeps outside the roughness sublayer of boundary layers (Raupach, 1981), leads to a reduction in w_s compared to w_{so}. Values of w_s/w_{so} for conditions where $d_p/\eta > 1$, s $\leq O(1)$, and when sediments remain in suspension (i.e., with R_* not deviating appreciably from unity) are not frequently considered despite their ubiquity in streams (Vanoni, 1984) and the atmosphere as summarized in Figure 1.

Compared to the aforementioned mechanisms, the unsteady vortex generation (Basset history forces) due to flow memory and the displacement of water with lower density than the grain density (virtual mass term) have received less attention in conventional suspended settling models such as Rouse's mean concentration profile and its associated R_*. As illustrated in Figure 1, the virtual mass term and Basset history forces can be separately significant across a wide range of particle sizes ($10^{-6} < d_p/\eta < 10^2$) and relative densities ($1 < \rho_p/\rho < 10^4$) when combining turbulent stream and atmospheric flows. This range covers clay, some micro-plastics, and various sands in water, as well as volcanic ash, snowflakes, and aerosols in the atmosphere and is thus pertinent to a plethora of geographical and atmospheric applications. This work investigates particle settling velocity in turbulent flows taking into account virtual mass and Basset history terms where they may be jointly and dynamically more significant compared to other processes. This range is $1 < \rho_p/\rho < 3$ (for virtual mass) and $0.1 < d_p/\eta < 10$ (for the Basset history) in Figure 1. Incorporating the effects of these two terms in a simplified mean sediment concentration budget provides a fresh perspective on ongoing controversies related to whether w_s/w_{so} exceeds unity or not

and whether $Sc = \nu_t/D_s$, a turbulent Schmidt number defined by the ratio of a turbulent viscosity (ν_t) and a particle turbulent diffusivity (D_s) also exceeds unity or not (Bombardelli & Moreno, 2012; van Rijn, 1984). Estimates of Sc inferred from measured mean sediment concentration profiles by fitting Rouse's solution often yield $Sc < 1$ whereas estimates of Sc from measured turbulent fluxes (sediments and momentum) and mean gradients yield $Sc > 1$ (Chauchat et al., 2022). Plausible connections between Sc, w_s/w_{so}, and the simultaneous role of the Basset history and virtual mass effects are the main novelty offered here for the regimes dominated by $1 < \rho_p/\rho < 3$ and $0.1 < d_p/\eta < 10$. These connections are explored in the inertial sublayer of boundary layers where the log-law reasonably describes the mean velocity profile and the second-order flow statistics do not vary appreciably with wall-normal distance.

2. Theory

Assuming a continuum representation for suspended sediment concentration or SSC (but see Bragg et al. (2021) for alternative approaches when this is not valid), the instantaneous sediment mass balance yields (Richter & Chamecki, 2018)

$$\frac{\partial C}{\partial t} + \frac{\partial}{\partial x_i}(V_i C) = D_m \frac{\partial^2 C}{\partial x_i \partial x_i}, \tag{1}$$

where t is time, C is the sediment concentration at position $\mathbf{x}$ (or x_i) and time t, D_m is the molecular diffusivity, V_i is the instantaneous advective velocity of the sediment grains, and $i = 1, 2, 3$ is a live index. In this notation, x_1 (or x), x_2 (or y), and x_3 (or z) represent the longitudinal, transverse, and vertical directions respectively. Upon using Reynolds averaging (indicated by overline), assuming stationary (i.e., $\partial\overline{(\cdot)}/\partial t = 0$) and planar homogeneous (i.e., $\partial\overline{(\cdot)}/\partial x = \partial\overline{(\cdot)}/\partial y = 0$) turbulent flow conditions with $V_3 = w_p$, Equation 1 simplifies to

$$\frac{\partial}{\partial z}\left(\overline{w_p}\,\overline{C} + \overline{w_p' C'}\right) = 0, \tag{2}$$

where transport by the molecular diffusion term $\left(D_m \partial\overline{C}/\partial z\right)$ is ignored relative to the turbulent flux $\overline{w_p' C'}$ after averaging, $w_p = w - w_s$ is the instantaneous net vertical advection velocity of the sediment particles and w_s is a terminal settling velocity of a single sediment particle and frames the scope of the work. Integration of Equation 2 with respect to z results in $\overline{w_p}\,\overline{C} + \overline{w_p' C'} = F_T$, where F_T is an integration constant that can be interpreted as the total sediment flux into or out of the control volume and is therefore determined by the boundary conditions. To evaluate F_T, the free water surface boundary is considered. At this boundary, it is assumed that no sediment additions occur, $\overline{C} = 0$, and $\nu_t = 0$ resulting in $F_T = 0$. This budget equation with $F_T = 0$ is the starting point of all operational models including Rouse's suspended sediment concentration (SSC) profile.

The sediment vertical velocity w_p is governed by a local force balance (Figure 1), and when the sediment grain size satisfies $d_p/\eta \ll 1$ and the particle Reynolds number $Re_p = |w(\mathbf{x}(t), t) - w_p| d_p/\nu$ is small (where ν is the fluid viscosity, and $\mathbf{x}(t)$ is the sediment position at time t), this force balance may be approximated by formulations discussed in Duman et al. (2016) and Maxey and Riley (1983) leading to

$$\begin{aligned}\frac{d}{dt} w_p = {} & \underbrace{s \frac{D}{Dt} w(\mathbf{x}(t), t)}_{flow\ \ acceleration} + \underbrace{\frac{3}{4} s \frac{C_d}{d_p} |w(\mathbf{x}(t), t) - w_p| \left[w(\mathbf{x}(t), t) - w_p\right]}_{drag} - \underbrace{g_o(1 - s)}_{gravity} \\ & - \underbrace{\frac{1}{2} s \frac{d}{dt}(w_p - w(\mathbf{x}(t), t))}_{virtual\ \ mass} - \underbrace{9 s \frac{1}{d_p} \sqrt{\frac{\nu}{\pi}} \int_0^t \frac{d(w_p - w(\mathbf{x}(t'), t'))/dt'}{\sqrt{t - t'}} dt'}_{Basset\ \ history},\end{aligned} \tag{3}$$

where $g_o = 9.8$ m s^{-2} is the gravitational acceleration, and C_d is a particle dimensionless drag coefficient. For $s = \rho/\rho_p \to 0$, this budget simplifies to $dw_p/dt = -g_o$ as expected. However, as $s \to 1$, the contribution of g_o can be ignored and the remaining terms including the flow acceleration, drag force, virtual mass, and the Basset history terms all become significant. To proceed further, an estimate of C_d is required. For smooth spherical grains of diameter d_p, C_d may be approximated as (Cheng, 2009)

$$C_d = \frac{24}{Re_p}(1 + 0.27 Re_p)^{0.43} + 0.47\left[1 - \exp(-0.04 Re_p)^{0.38}\right]. \tag{4}$$

In Equation 4, the $C_d = 24/Re_p$ is the Stokes drag coefficient valid for small Re_p, and the remaining terms in Equation 4 are additive and multiplicative corrections to the Stokes coefficient. When the Stokes contribution in Equation 4 is dominant, the drag force in Equation 3 scales as $d_p^{-2}\left[w(\mathbf{x}(t),t) - w_p\right]$.

The Basset history term, which arises due to a temporal delay and unsteadiness of the boundary layer developing on the moving grain, is much more difficult to represent in sign and magnitude. However, inspection of Equation 3 is suggestive that the magnitude of the Basset history scales as d_p^{-1}. Hence, the ratio of Basset history to drag force scales with d_p, and the Basset term can only be ignored if d_p/η is very small, where η is presumed to be the smallest scale of motion where turbulence remains significant. Direct numerical simulation (DNS) studies have shown that the behavior of Basset history term may be approximated as being proportional to the drag force according to Daitche (2015), Daitche and Tél (2011), and Guseva et al. (2016)

$$\frac{Basset\ \ history\ \ term}{Drag\ \ \ force\ \ term} = \alpha_\eta\left(\frac{d_p}{\eta}\right), \tag{5}$$

where α_η is a similarity coefficient of order unity (Daitche, 2015; Guseva et al., 2016). The sign of the Basset history is not obvious but evidence also suggests that (at least on average) it reduces the slip velocity between fluid and particle grains implying Re_p is reduced and C_d is enhanced by this term (Daitche, 2015; Guseva et al., 2016). Accordingly, the particle acceleration in Equation 3 simplifies to

$$\left(1+\frac{1}{2}s\right)\frac{d}{dt}w_p = \frac{3s}{2}\frac{D}{Dt}w(\mathbf{x}(t),t) + \frac{3}{4}s\frac{1}{d_p}C_d\left[1+\alpha_\eta\left(\frac{d_p}{\eta}\right)\right]|w(\mathbf{x}(t),t) - w_p|\left[w(\mathbf{x}(t),t) - w_p\right] - g_o(1-s). \tag{6}$$

Equation 6 can be expressed as (Druzhinin, 1995; Good et al., 2014; Kawanisi & Shiozaki, 2008),

$$\frac{d}{dt}w_p = \lambda\frac{Dw}{Dt} + \frac{1}{\tau_p}\left[w(\mathbf{x}(t),t) - w_p\right] - g, \tag{7}$$

where the characteristic particle timescale τ_p, the modified gravitational acceleration and a density modification coefficient λ are now defined as

$$\tau_p^{-1} = \frac{1}{2}\lambda\frac{C_d}{d_p}\left[1+\alpha_\eta\left(\frac{d_p}{\eta}\right)\right]|w(\mathbf{x}(t),t) - w_p|, \qquad g = g_o\left(\frac{2-2s}{2+s}\right), \qquad \lambda = \left(\frac{3s}{2+s}\right). \tag{8}$$

The τ_p now includes the effect of the Basset history term through a finite α_η and the added virtual mass in λ. When d_p/η is sufficiently small, the Basset history term can be ignored. The Basset history and virtual mass jointly act to increase the effective C_d but those terms are associated with different mechanisms when compared to averaging a non-linear form of C_d over variations in $|w(\mathbf{x}(t),t) - w_p|$. Moreover, the g is also reduced from g_o by $(2-2s)/(2+s)$ due to $s < 1$ as is the case for sedimentation.

To link w_p to w in Equation 7, a small Stokes number ($St_+ = \tau_p u_*/H$, H is a large length scale) perturbation analysis (Druzhinin, 1995; Ferry & Balachandar, 2001; Maxey & Riley, 1983) is used and shown in Supporting Information S1. The suitability of the small St_+ assumption when the target variable is $\overline{C}(z)$ within the log-layer will be discussed later. As a result, the sediment settling velocity (dimensional) can be derived as a function of the fluid vertical velocity and particle time scale using,

$$w_p = w - \tau_p\, g + (\lambda - 1)\tau_p\frac{Dw}{Dt} + \tau_p^2 g\frac{\partial w}{\partial z}. \tag{9}$$

The new characteristic sediment settling velocity w_s emerges as a zeroth order estimation of the sediment settling velocity in turbulent flow and is now presented as

$$w_s = \tau_p\, g = w_{so}\left[\frac{1}{\alpha_\eta\,(d_p/\eta)+1}\right]^{1/2}, \quad \text{where } w_{so} = \frac{1}{C_d}\frac{4-4s}{3s}\frac{g_o\, d_p}{|w - w_p|} = 2\sqrt{\left(\frac{1-s}{3s}\right)\frac{g_o d_p}{C_d}}. \tag{10}$$

The outcome in Equation 10 suggests that $w_s/w_{so} \to 1$ when $d_p/\eta \to 0$. Moreover, w_s is reduced with increasing d_p/η. The virtual mass and the Basset history terms appear to act in concert to reduce w/w_{so} from unity. Substituting Equation 9 into Equation 2 and performing the Reynolds averaging operation on each term, a sediment mass budget can be obtained as

$$w_{so}\overline{C} - \overline{w'C'} - (w_{so} - w_s)\overline{C} = \tau_p\left[\frac{1}{2}(\lambda - 1)\overline{C}\frac{\partial\sigma_w^2}{\partial z} + (\lambda - 1)\overline{\left(C'\frac{Dw'}{Dt}\right)} + w_s\overline{C'\frac{\partial w'}{\partial z}}\right], \quad (11)$$

where $\sigma_w = \sqrt{w'^2}$ is the fluid vertical velocity standard deviation. The terms on the right-hand side of Equation 11 are respectively produced from the turbophoretic effect and finite particle inertia as discussed in Supporting Information S1. This latter effect indirectly accounts for preferential sweeping (especially with increasing St_+). The term $(w_{so} - w_s)\overline{C}$ on the left-hand side of Equation 11 is the missing flux in Rouse's analysis correcting the still-water gravitational term attributed here to the Basset history and virtual mass. A result similar to Equation 11 was previously derived (Richter & Chamecki, 2018); however, this prior analysis did not include the Basset history, virtual mass and the fluid acceleration terms.

To recap, when using Rouse's analysis, the following approximations are invoked: $w_{so} = w_s$ and all the terms on the right-hand side of Equation 11 are ignored ($\tau_p \to 0$). The Basset history term is expected to be significant when d_p/η is not very small, and the effects of virtual mass are large when s is close but below unity. Equation 11 suggests that this residual flux arising from the difference between the turbulent settling velocity and still water settling velocity is given as

$$R_f = \frac{w_{so} - w_s}{w_{so}} = 1 - \sqrt{\theta_{cd}}\left[\frac{1}{\alpha_\eta\,(d_p/\eta) + 1}\right]^{1/2}, \quad (12)$$

where $\theta_{cd} = C_d(w_s)/C_d(w_{so})$ is an adjustment coefficient due to the variations of the differences in drag coefficients in still water and turbulence. For inhomogeneous turbulent flows where $d\sigma_w^2/dz$ can be large (e.g., turbulent boundary layers near the wall or in the outer region), it may be argued that the turbophoretic effect on the right-hand side of Equation 11 must be included given that it scales with $\overline{C}$. However, in the inertial region (i.e., where the log layer for the mean velocity is expected to hold), the turbophoretic effect is minor because σ_w/u_* is roughly constant in z. The last two terms in Equation 11 representing turbulent sweeping effects are rarely quantitatively scaled in the literature due to their intractability. Thus, as a logical starting point, they are temporarily dropped here and the focus is given to only the Basset history and virtual mass terms. The budget in Equation 11 that ignores the right-hand side but maintains the residual flux R_f is now used to examine the outcome of a number of laboratory experiments that report $w_s/w_{so} < 1$ for $d_p/\eta > 1$ and $\rho_p/\rho \in [1, 3]$ within the inertial sublayer.

3. Experiments and Model Comparison

Three different laboratory experiments are used and interpreted using Equation 11. The first experiment is presented in Revil-Baudard et al. (2015) and is labeled as RB15 while the other two experiments are presented in Shen and Lemmin (1999) and are labeled as SLR1 and SLR2. These experiments are selected because flow and sediment concentration statistics were publicly available. Briefly, the experiments were conducted in rectangular channels with width B and bed slope S_o for steady and uniform flow characterized by a constant flow rate Q. Sidewall friction was presumed to be small compared to bed friction so that the water level H reasonably approximates the hydraulic radius R_H. A partial justification for setting $R_H = H$ is not based on geometry because H/B is not an order of magnitude smaller than unity in all experiments. It is based on the fact that the bed is covered with sediments and is much rougher than the side channels (usually smooth glass or plastic to permit optical access). Thus, $u_*^2 = g_o S_o H$ and the bulk velocity $U_b = Q/(BH)$. The bulk turbulent kinetic energy dissipation rate can now be determined from bulk variables as $\epsilon_b = U_b(g_o S_o) = (U_b/H)u_*^2$ enabling an estimate of a bulk Kolmogorov micro-scale eddy size $\eta_b = \left(\nu^3/\epsilon_b\right)^{1/4}$ to be compared with reported grain diameter d_p without any z dependency for convenience (S. Li et al., 2022). In all model calculations, the local $\epsilon(z)$ is used in the estimation of $\eta(z) = \left[\nu^3/\epsilon(z)\right]^{1/4}$. Near the channel bed and in the inertial (or log-layer), $\epsilon(z)/\epsilon_b > 1$ so that $\eta(z)/\eta_b < 1$. The η_b must be viewed as an upper limit on the Kolmogorov microscale and d_p/η_b as a lower limit for the experiment at hand when evaluating the Basset history in the target region. The bulk conditions across experiments are compared and summarized in Table S2 in Supporting Information S1. All three experiments have commensurate U_b, u_*, and η_b. The computed $R_* = w_o/(\kappa u_*) > 2.5$ using the reported measured settling velocity in still water (labeled as w_o) for RB15, where $\kappa = 0.4$ is the von Kármán constant. However, the computed R_* for SLR1 and SLR2 were consistent with a 100% suspended sediment and wash-load classification (i.e., $R_* \in [0.5, 1.2]$). This outcome alone hints that adjustments to R_* (i.e., reduced settling velocity) must be invoked to maintain suspension in RB15. It is also known that the mean settling velocity of sediments may be reduced by hindrance effects,

caused by obstacles or other particles in the fluid that impede their motion. However, recent analysis by Chauchat et al. (2022) using their RB15 data showed that such hindrance mechanism may not be sufficient to account for the observed retardation effects. Therefore, particle-particle hindrance effects are not considered.

Common issues in turbulent flux measurements are short sampling duration and small sampling frequency f_s. To explore these two effects on the data here, especially RB15, an idealized co-spectrum of the turbulent sediment flux was assumed and featured in Supporting Information S1. Key findings from this supplementary are that the combined effects of these two corrections appear to be large (as high as a factor of 2) but their leading order effect can be accommodated in the comparisons presented next, at least for RB15 where all the necessary data are available. The corrected (where possible) and uncorrected turbulent fluxes are presented in the figures for RB15. The reported profiles of mean velocity (U), $-\overline{w'u'}$, mean sediment concentration $\left(\overline{C}\right)$, $\overline{w'C'}$, and $\sigma_w = \sqrt{\overline{w'^2}}$ (Revil-Baudard et al., 2015; Shen & Lemmin, 1999) and summarized by Chauchat et al. (2022) are shown in Figure 2. The shaded area in these figures indicates the inertial (or log-law) region. This region is characterized by measured $\gamma = \sigma_w/u_*$ not varying appreciably with z but different across experiments due to H/B restrictions as noted earlier. Hence, turbophoresis may be ignored in this layer. When $H/B \to 0$ (e.g., a near-neutral atmospheric surface layer flows), $\gamma = 1.2 - 1.3$ and is larger than the reported γ in the experiments here. Only RB15 reported a γ of order unity. The measured still water settling velocity (i.e., w_o) in all three studies, the computed settling velocity w_{so}, and the characteristic turbulent settling velocity w_s are highlighted in Figure 2. The $w_o/w_{so} < 1$ when w_{so} is computed for spherical smooth grains as noted in previous studies (Cheng, 1997).

When $\alpha_\eta = 0.7$ predetermined from DNS (Dai et al., 2016; Daitche, 2015; Guseva et al., 2016), good agreement (a maximal deviation of 25%) between the settling flux and turbulent flux can indeed be achieved except for RB15. The RB15 data set can also be matched if the turbulent flux is corrected (e.g., with $\overline{w'C'}_c$ or α_η is fitted as 2.0 without correction using $\overline{w'C'}$). It is noted that the co-spectral correction to the turbulent flux in RB15 are large (see Supporting Information S1) and may be an overestimate of the correction magnitude. Furthermore, the measured turbulent flux, the corrected turbulent flux, and the gravitational settling flux in Equation 11 are separately examined (see Supporting Information S1) implying that the inclusion of the Basset history term offers a plausible explanation to reduced sediment settling velocity in turbulent flows for all these experiments. However, for $\alpha_\eta = 0.7$, the flux budget is indeed matched after co-spectral corrections are applied to the turbulent flux for RB15. Likewise, an $\alpha_\eta = 0.7$ reasonably matches the other data sets (original fluxes) though co-spectral corrections could not be determined for SLR1 and SLR2. The more interesting feature here is that the computed w_s from Equation 10 with $\alpha_\eta = 0.7$ remains significantly smaller compared to w_o. This finding supports the conjecture that turbulence indeed reduces the sediment settling with the highest retardation occurring for the largest d_p. Equation 10 attributes this reduction to the Basset history and the added virtual mass terms. For $z/H < 0.18$, inferred w_s appears to be not constant in two experiments (SLR1 and SLR2), which may be indicative that other effects are significant near the wall such as turbophoresis or particle-particle interaction due to the high concentration near the bed.

4. Discussion

4.1. Revisiting the Turbulent Schmidt Number

The turbulent Schmidt number can be expressed as

$$Sc = \frac{\nu_t}{D_s} = \frac{-\overline{w'u'}}{-\overline{w'C'}} \frac{d\overline{C}/dz}{d\overline{u}/dz}. \tag{13}$$

The inferred Sc directly from measurements is shown in Figure 2 in the inertial layer. As shown in panel (i) of Figure 2, the $Sc = 3.5$ appears constant for all experiments in the inertial layer. An $Sc > 1$ was suggested to counter Rouse's original model interpretation (Rouse, 1937; van Driest, 1956). The original outcome that the turbulent $Sc < 1$ (traditionally denoted as β^{-1} in many studies) from Rouse's mean concentration profile (Rouse, 1937; van Driest, 1956) can be explored using R_f. Adopting van Rijn's formula (van Rijn, 1984), a definition of a "modified" Schmidt number represented by β^{-1} was introduced and may be expressed as

$$\beta^{-1} = \frac{\overline{w'u'}}{w_{so}\overline{C}} \frac{d\overline{C}/dz}{d\overline{u}/dz} = Sc \frac{\overline{w'C'}}{w_{so}\overline{C}} = Sc(1 - R_f), \tag{14}$$

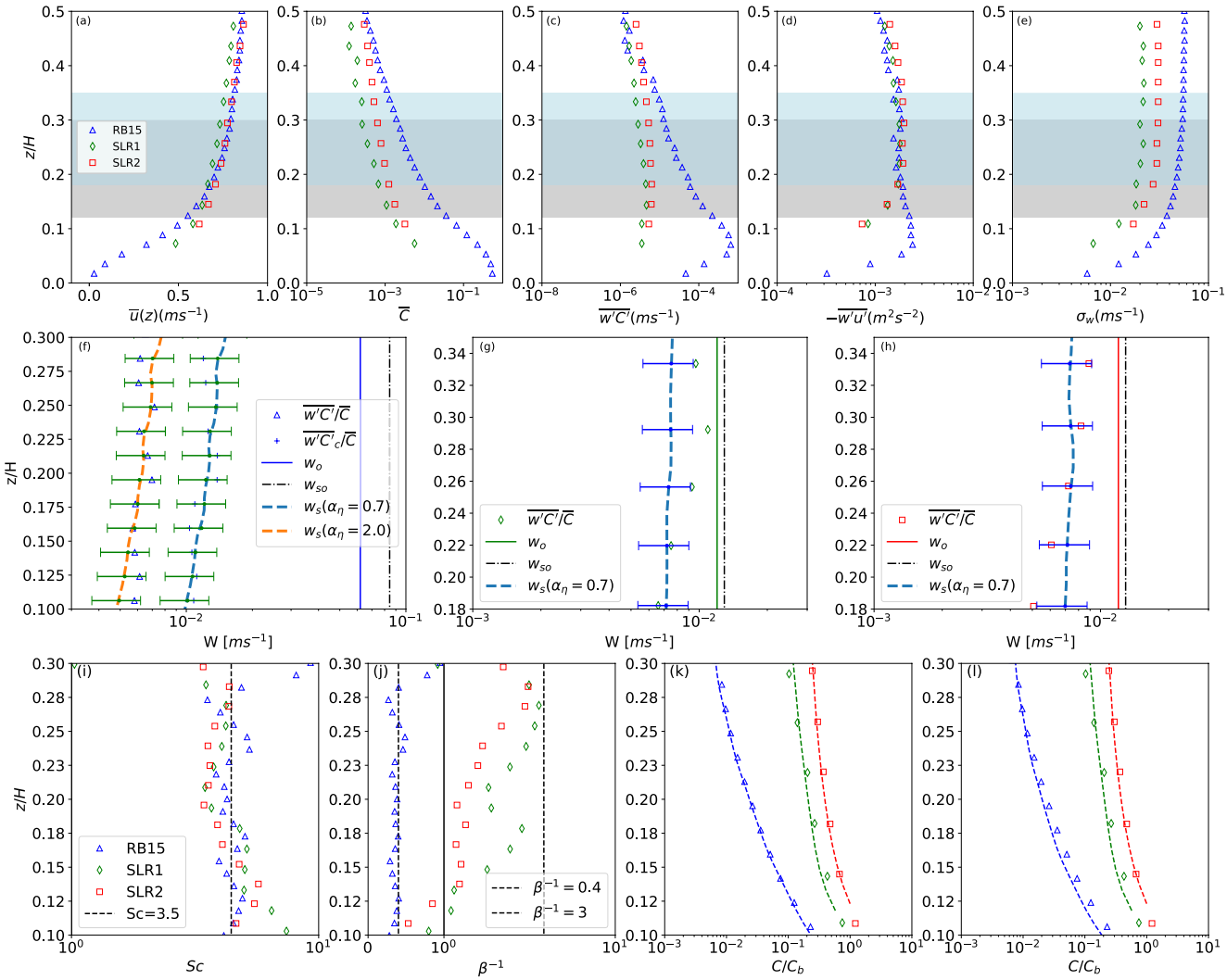

Figure 2. Top panel (a–e): The reported profiles of turbulent flow and sediment statistics from Revil-Baudard et al. (2015), Chauchat et al. (2022) (blue color, RB15), and Runs 1 (green color, SLR1) and 2 (red color, SLR2) from Shen and Lemmin (1999). Different data sets are marked in different colors in a consistent manner throughout all the figures. The inertial layers are also highlighted in light gray ($z/H > 0.12$ but <0.3 for RB15) and light blue ($z/H > 0.18$ but <0.3 for SLR1 and SLR2). Middle panel (f–h): The three subplots show the computed and reported settling velocities (w) corresponding to RB15, SLR1, and SLR2 respectively. In each subplot, the four settling velocities are (i) computed turbulent settling velocity w_s from Equation 10 with $\alpha_\eta = 0.7$ from Direct numerical simulation (the error bar shows a 25% deviation off the mean), (ii) the settling velocity w_{so} from Equation 10 in black dot-dash lines, (iii) the experimentally reported still water settling velocity w_o in solid line and (iv) the settling velocity from measurements using raw $\left(\overline{w'C'}/\overline{C}\right)$ and co-spectrally corrected turbulent flux values (for RB15 only) $\left(\overline{w'C'}_c/\overline{C}\right)$. Bottom panel (i–l): Comparison of different turbulent Schmidt numbers (Sc) computed from Equation 13 and using Equation 14. For the overall estimates of Sc and β^{-1} reported in Table S2 in Supporting Information S1, fitting measured (symbols) to modeled (lines) $C(z)$ is used. In panels (k–l) the dashed lines are the predictions of the SSC. (k) Shows the revised Rouse model that accommodates the Basset history and virtual mass terms with no fitting parameters, while (l) shows the best-fit of the original Rouse equation to data.

where $R_f = 1 - w_s/w_{so}$ is the residual flux when the Basset history and virtual mass are included in the particle force balance. As shown from Equation 14, the turbulent Schmidt number β^{-1} used in Rouse's formula can now be viewed as a product of two terms: a "true" Schmidt number modified by a factor $(1 - R_f)$ to accommodate the missing forces (here, the virtual mass and Basset history). The plot of β^{-1} is shown in panel (j) of Figure 2 where the RB15 data are smaller than unity ($R_f > 0$) while the SLR1 and SLR2 are not (discussed later). The "controversy" about $Sc > 1$ can be addressed when noting that the reported β^{-1} is not the actual turbulent Schmidt number as may be inferred from Equation 13. The β^{-1} must be interpreted as a characteristic turbulent Schmidt number "pinned" to a settling flux based on the still water settling velocity instead of a turbulence-reduced settling velocity.

It is noted that an $Sc > 1$ (as is the case here) qualitatively agrees with the "crossing-trajectories" argument developed for heavy particles in turbulent flows (Csanady, 1963; Stout et al., 1995; Wells & Stock, 1983). The crossing trajectories argument suggests that heavy particles will move from highly correlated regions in the flow to less correlated regions when their trajectories intersect those of fluid elements, typically due to the influence of gravity. This phenomenon leads to an increase in flow diffusivity and a decrease in sediment diffusivity, resulting in $Sc > 1$. This behavior is analogous to the Basset history effect, which causes the generation of unsteady vortices and added mass due to the displacement of particles and water within the local region bounded by the particle volumes.

4.2. A Re-Examination of Rouse's Budget

The improved skill of accommodating the Basset history and virtual mass in the SSC budget is now evaluated in terms of predicting the $\overline{C}(z)$ with z/H. Numerical integration of Equation 15 is used to derive the mean SSC. The measured flow statistics profiles were digitized and used in the computation of $\overline{C}(z)$. The depth integration to derive the SSC for the two models is given by,

$$\begin{aligned}\frac{\overline{C}(z)}{\overline{C}_b} &= \exp\left[\int_{z_b}^{z}\left(\beta^{-1}\frac{w_{so}}{\overline{u'w'}}\frac{d\overline{u}}{dz}\right)dz\right], \quad \text{original Rouse budget;}\\ \frac{\overline{C}(z)}{\overline{C}_b} &= \exp\left[\int_{z_b}^{z}\left(Sc(1-R_f)\frac{w_{so}}{\overline{u'w'}}\frac{d\overline{u}}{dz}\right)dz\right], \quad \text{revised Rouse budget.}\end{aligned} \tag{15}$$

To optimize Rouse's original concentration profile solution (i.e., $R_f = 0$), β^{-1} was set as a "free parameter" in Equation 15. For the revised Rouse budget, no fitting was necessary provided Sc was externally set. The R_f was computed (and varied with z) using the reported s for the virtual mass and the modeled Basset history term with $\alpha_\eta = 0.7$ (see Figure 2) and $Sc = 3.5$ determined from the experiments shown in Figure 2. The predicted SSC profiles using the original Rouse solution and the present method are shown in Figure 2. The comparison features the optimized β^{-1} summarized in Table S2 in Supporting Information S1.

Figure 2 demonstrates that predicted $\overline{C}(z)$ profiles agree with observed values for both formulations though minor improvements are noted for the proposed formulation that includes the z dependency of R_f. Free-fitting β^{-1} makes the modeled SSC profiles match measurements even though the assumption that the turbulent flux is balanced by the still water settling flux is incomplete. This agreement between data and the original Rouse model may be due to the fact that d_p/η is insensitive to small variations in z within the log-layer as η scales only as $z^{1/4}$ (i.e., sub-unity exponent). Hence, different grain sizes or flow conditions simply increase the variability in β^{-1} when fitting the original Rouse model to measured $\overline{C}(z)$ but the $\overline{C}(z)$ dependency on z is not significantly altered. Table S2 in Supporting Information S1 makes clear why prior studies reported an $Sc = \beta^{-1} < 1$. Computing β^{-1} by fitting Rouse's formula to measured $\overline{C}(z)$ and then setting $Sc = \beta^{-1}$ yields an apparent $Sc < 1$. The inferred β^{-1} from fitting Rouse's profile to concentration data all result in $\beta^{-1} < 1$ whereas computed β^{-1} from data in Figure 2 exceeds unity for two experiments (SLR1 and SLR2). Accounting for R_f variations in z and using $Sc = 3.5$ yields good agreement between measured and modeled $\overline{C}(z)$ for the same data sets.

4.3. Model Limitation

The model assumptions warrant further scrutiny. First, the particle equation of motion (i.e., Equation 3) was derived from a force balance on a single grain assuming the grain is finite in size but small in diameter (i.e., $d_p/\eta \leq 1$), spherical and rigid, and experiencing a small particle Reynolds number. Moreover, a solution to the particle equation of motion was derived assuming that the particle Stokes number $St_+ = \tau_p u_*/H$ is small. The data in Table S2 in Supporting Information S1 shows that the particles in all three experiments have values $St_+ = O(10^{-3})$ and therefore the assumption is clearly validated. This assertion remains true even when H is replaced by z in the St_+ expression for z within the log-layer (order 0.1 H).

Returning to the case where $d_p/\eta_b > 1$, it is more crucial that d_p be much smaller than the flow scales influencing $\overline{C}(z)$. Thus, it is the large scales (i.e., z), not the Kolmogorov scales, that predominantly affect the behavior of $\overline{C}(z)$. That is, Equation 3 still applies for modeling $\overline{C}(z)$ in the log-layer, especially when $d_p/z \ll 1$. This finding is supported by Costa et al. (2020) who showed that away from the wall ($z/H > 0.2$), finite-size particles' behavior

agree with point-particle results from Equation 3. In the experiments here, d_p/z remains much smaller than unity within the log-layer suggestive that Equation 3 can be used for predicting $\overline{C}(z)$ in that layer. Finally, the model emphasizes the significance of the Basset history in the experiments here due to the non-negligible value of d_p/η. It could be argued that the Faxen correction terms in the particle equation of motion (i.e., Equation 3) must also be employed when d_p/η is finite (Maxey & Riley, 1983). The relevance of those corrections was explored in a number of studies (Dai et al., 2016; Daitche, 2015) and they were deemed minor for the parameter range here. The inclusion of the Basset history and added mass terms suffice to explain the reduction in the settling velocity relative to its still value hinting that the omission of the Faxen corrections is acceptable in the log-region. More evaluations are also presented in the Supporting Information S1.

5. Conclusion

The work here focused on the particle setting velocity in a turbulent flow for the cases where (a) the diameter of sediment particles is of the same order as or exceeds the Kolmogorov micro-scale, and (b) the particle density is not substantially different from (but exceeds) that of the fluid. It was shown that for such ubiquitous conditions in many geophysical flows, an "upgrade" to the current formulation of the sediment settling velocity is necessary. The proposed upgrade incorporates the simultaneous effects of the Basset history term and virtual mass and leads to particle settling velocities smaller than their still water counterparts. These two effects also elucidate the observed variability in the turbulent Schmidt number, which is commonly inferred by fitting measured mean sediment concentration profiles to Rouse's formula. The turbulent Schmidt number derived from fitting Rouse's profile to measurements a priori assumes that $w_s/w_{so} = 1$. Hence, deviations from such an assumption can be erroneously attributed to a turbulent Schmidt effect.

Future effort seeks to expand this model to include (a) inhomogeneous flow conditions where turbophertic effects can be significant (e.g., near boundaries or free water interfaces), (b) other phoretic effects such as thermophoresis needed in stratified atmospheric flow studies, and (c) finite particle inertia where preferential sweeping effects can become significant. Moreover, for many other applications such as dispersion of micro-plastics, relaxing the rigid spherical assumption is also needed. To accomplish these revisions requires dedicated (and expensive) direct numerical simulations, a task which must be kept for the future.

Data Availability Statement

All the data used are from published sources (Chauchat et al., 2022) and no new data were produced from this work.

Acknowledgments
Support from the U.S. National Science Foundation (NSF-AGS-2028633), the Department of Energy (DE-SC0022072), and the Army Research Office (W911NF-22-2-0222) is acknowledged.

References

Akutina, Y., Revil-Baudard, T., Chauchat, J., & Eiff, O. (2020). Experimental evidence of settling retardation in a turbulence column. *Physical Review Fluids*, *5*(1), 014303. https://doi.org/10.1103/physrevfluids.5.014303

Alonso-González, I. J., Arístegui, J., Lee, C., Sanchez-Vidal, A., Calafat, A., Fabrés, J., et al. (2010). Role of slowly settling particles in the ocean carbon cycle. *Geophysical Research Letters*, *37*(13), L13608. https://doi.org/10.1029/2010GL043827

Bombardelli, F., & Moreno, P. (2012). Exchange at the bed sediments-water column interface. In C. Gualtieri, & D. T. Mihailovic (Eds.), *Fluid mechanics of environmental interfaces* (2nd ed., pp. 221–253).

Bragg, A. D., Richter, D. H., & Wang, G. (2021). Mechanisms governing the settling velocities and spatial distributions of inertial particles in wall-bounded turbulence. *Physical Review Fluids*, *6*, 064302. https://doi.org/10.1103/physrevfluids.6.064302

Chauchat, J., Hurther, D., Revil-Baudard, T., Cheng, Z., & Hsu, T.-J. (2022). Controversial turbulent Schmidt number value in particle-laden boundary layer flows [Dataset]. Physical Review Fluids, *7*(1), 014307. https://doi.org/10.5281/zenodo.5765565

Cheng, N.-S. (1997). Simplified settling velocity formula for sediment particle. *Journal of Hydraulic Engineering*, *123*(2), 149–152. https://doi.org/10.1061/(asce)0733-9429(1997)123:2(149)

Cheng, N.-S. (2009). Comparison of formulas for drag coefficient and settling velocity of spherical particles. *Powder Technology*, *189*(3), 395–398. https://doi.org/10.1016/j.powtec.2008.07.006

Costa, P., Brandt, L., & Picano, F. (2020). Interface-resolved simulations of small inertial particles in turbulent channel flow. *Journal of Fluid Mechanics*, *883*, A54. https://doi.org/10.1017/jfm.2019.918

Csanady, G. (1963). Turbulent diffusion of heavy particles in the atmosphere. *Journal of the Atmospheric Sciences*, *20*(3), 201–208. https://doi.org/10.1175/1520-0469(1963)020<0201:tdohpi>2.0.co;2

Dai, Z., Fagherazzi, S., Mei, X., & Gao, J. (2016). Decline in suspended sediment concentration delivered by the Changjiang (Yangtze) river into the East China sea between 1956 and 2013. *Geomorphology*, *268*, 123–132. https://doi.org/10.1016/j.geomorph.2016.06.009

Daitche, A. (2015). On the role of the history force for inertial particles in turbulence. *Journal of Fluid Mechanics*, *782*, 567–593. https://doi.org/10.1017/jfm.2015.551

Daitche, A., & Tél, T. (2011). Memory effects are relevant for chaotic advection of inertial particles. *Physical Review Letters*, *107*(24), 244501. https://doi.org/10.1103/physrevlett.107.244501

Davarpanah Jazi, S., & Wells, M. G. (2016). Enhanced sedimentation beneath particle-laden flows in lakes and the ocean due to double-diffusive convection. *Geophysical Research Letters*, *43*(20), 10883–10890. https://doi.org/10.1002/2016GL069547

Dey, S. (2014). *Fluvial hydrodynamics: Hydrodynamic and sediment transport phenomena* (687 pp.). Springer.

Dietrich, W. E. (1982). Settling velocity of natural particles. *Water Resources Research*, *18*(6), 1615–1626. https://doi.org/10.1029/wr018i006p01615

Druzhinin, O. (1995). On the two-way interaction in two-dimensional particle-laden flows: The accumulation of particles and flow modification. *Journal of Fluid Mechanics*, *297*, 49–76. https://doi.org/10.1017/s0022112095003004

Duman, T., Trakhtenbrot, A., Poggi, D., Cassiani, M., & Katul, G. G. (2016). Dissipation intermittency increases long-distance dispersal of heavy particles in the canopy sublayer. *Boundary-Layer Meteorology*, *159*(1), 41–68. https://doi.org/10.1007/s10546-015-0112-y

Ferry, J., & Balachandar, S. (2001). A fast Eulerian method for disperse two-phase flow. *International Journal of Multiphase Flow*, *27*(7), 1199–1226. https://doi.org/10.1016/s0301-9322(00)00069-0

Fornari, W., Picano, F., Sardina, G., & Brandt, L. (2016). Reduced particle settling speed in turbulence. *Journal of Fluid Mechanics*, *808*, 153–167. https://doi.org/10.1017/jfm.2016.648

Good, G., Ireland, P., Bewley, G., Bodenschatz, E., Collins, L., & Warhaft, Z. (2014). Settling regimes of inertial particles in isotropic turbulence. *Journal of Fluid Mechanics*, *759*, R3. https://doi.org/10.1017/jfm.2014.602

Guseva, K., Daitche, A., Feudel, U., & Tél, T. (2016). History effects in the sedimentation of light aerosols in turbulence: The case of marine snow. *Physical Review Fluids*, *1*(7), 074203. https://doi.org/10.1103/physrevfluids.1.074203

Huai, W., Li, S., Katul, G., Liu, M.-Y., & Yang, Z.-H. (2021). Flow dynamics and sediment transport in vegetated rivers: A review. *Journal of Hydrodynamics*, *33*(3), 400–420. https://doi.org/10.1007/s42241-021-0043-7

Huang, Y., Kok, J. F., Kandler, K., Lindqvist, H., Nousiainen, T., Sakai, T., et al. (2020). Climate models and remote sensing retrievals neglect substantial desert dust asphericity. *Geophysical Research Letters*, *47*(6), e2019GL086592. https://doi.org/10.1029/2019GL086592

Kawanisi, K., & Shiozaki, R. (2008). Turbulent effects on the settling velocity of suspended sediment. *Journal of Hydraulic Engineering*, *134*(2), 261–266. https://doi.org/10.1061/(asce)0733-9429(2008)134:2(261)

Li, J., & Osada, K. (2007). Preferential settling of elongated mineral dust particles in the atmosphere. *Geophysical Research Letters*, *34*(17), L17807. https://doi.org/10.1029/2007GL030262

Li, S., Bragg, A. D., & Katul, G. (2022). A co-spectral budget model links turbulent eddies to suspended sediment concentration in channel flows. *Water Resources Research*, *58*(3), e2021WR031045. https://doi.org/10.1029/2021wr031045

Maxey, M. R. (1987). The gravitational settling of aerosol particles in homogeneous turbulence and random flow fields. *Journal of Fluid Mechanics*, *174*, 441–465. https://doi.org/10.1017/S0022112087000193

Maxey, M. R., & Riley, J. J. (1983). Equation of motion for a small rigid sphere in a nonuniform flow. *The Physics of Fluids*, *26*(4), 883–889. https://doi.org/10.1063/1.864230

Mora, D. O., Obligado, M., Aliseda, A., & Cartellier, A. (2021). Effect of Re and Rouse numbers on the settling of inertial droplets in homogeneous isotropic turbulence. *Physical Review Fluids*, *6*(4), 044305. https://doi.org/10.1103/physrevfluids.6.044305

Raupach, M. (1981). Conditional statistics of Reynolds stress in rough-wall and smooth-wall turbulent boundary layers. *Journal of Fluid Mechanics*, *108*, 363–382. https://doi.org/10.1017/s0022112081002164

Revil-Baudard, T., Chauchat, J., Hurther, D., & Barraud, P.-A. (2015). Investigation of sheet-flow processes based on novel acoustic high-resolution velocity and concentration measurements. *Journal of Fluid Mechanics*, *767*, 1–30. https://doi.org/10.1017/jfm.2015.23

Richter, D., & Chamecki, M. (2018). Inertial effects on the vertical transport of suspended particles in a turbulent boundary layer. *Boundary-Layer Meteorology*, *167*(2), 235–256. https://doi.org/10.1007/s10546-017-0325-3

Rouse, H. (1937). Modern conceptions of the mechanics of fluid turbulence. *Transactions of the American Society of Civil Engineers*, *102*(1), 463–505. https://doi.org/10.1061/taceat.0004872

Scollo, S., Coltelli, M., Prodi, F., Folegani, M., & Natali, S. (2005). Terminal settling velocity measurements of volcanic ash during the 2002–2003 Etna eruption by an X-band microwave rain gauge disdrometer. *Geophysical Research Letters*, *32*(10), L10302. https://doi.org/10.1029/2004GL022100

Shen, C., & Lemmin, U. (1999). Application of an acoustic particle flux profiler in particle laden open-channel flow. *Journal of Hydraulic Research*, *37*(3), 407–419. https://doi.org/10.1080/00221686.1999.9628256

Shu, A., & Fei, X. (2008). Sediment transport capacity of hyperconcentrated flow. *Science in China Series G: Physics, Mechanics and Astronomy*, *51*(8), 961–975. https://doi.org/10.1007/s11433-008-0108-4

Squires, K. D., & Eaton, J. K. (1991). Preferential concentration of particles by turbulence. *Physics of Fluids A: Fluid Dynamics*, *3*(5), 1169–1178. https://doi.org/10.1016/0301-9322(94)90072-8

Stout, J., Arya, S., & Genikhovich, E. (1995). The effect of nonlinear drag on the motion and settling velocity of heavy particles. *Journal of the Atmospheric Sciences*, *52*(22), 3836–3848. https://doi.org/10.1175/1520-0469(1995)052<3836:teondo>2.0.co;2

Tom, J., & Bragg, A. D. (2019). Multiscale preferential sweeping of particles settling in turbulence. *Journal of Fluid Mechanics*, *871*, 244–270. https://doi.org/10.1017/jfm.2019.337

Tom, J., Carbone, M., & Bragg, A. D. (2022). How does two-way coupling modify particle settling and the role of multiscale preferential sweeping? *Journal of Fluid Mechanics*, *947*, A7. https://doi.org/10.1017/jfm.2022.615

van Driest, E. (1956). On turbulent flow near a wall. *Journal of the Aeronautical Sciences*, *23*(11), 1007–1011. https://doi.org/10.2514/8.3713

Vanoni, V. A. (1984). Fifty years of sedimentation. *Journal of Hydraulic Engineering*, *110*(8), 1021–1057. https://doi.org/10.1061/(asce)0733-9429(1984)110:8(1021)

van Rijn, L. C. (1984). Sediment transport, part II: Suspended load transport. *Journal of Hydraulic Engineering*, *110*(11), 1613–1641. https://doi.org/10.1061/(asce)0733-9429(1984)110:11(1613)

Van Rijn, L. C. (1993). Principles of sediment transport in rivers. In *Estuaries and Coastal Seas*. Aqua Publications.

von Kármán, T. (1934). Some aspects of the turbulence problem. In *Proceedings of the fourth international congress of applied mechanics* (pp. 54–91).

Wang, L.-P., & Maxey, M. R. (1993). Settling velocity and concentration distribution of heavy particles in homogeneous isotropic turbulence. *Journal of Fluid Mechanics*, *256*, 27–68. https://doi.org/10.1017/S0022112093002708

Wells, M., & Stock, D. (1983). The effects of crossing trajectories on the dispersion of particles in a turbulent flow. *Journal of Fluid Mechanics*, *136*(1), 31–62. https://doi.org/10.1017/s0022112083002049

Wu, W., & Wang, S. S. (2006). Formulas for sediment porosity and settling velocity. *Journal of Hydraulic Engineering*, *132*(8), 858–862. https://doi.org/10.1061/(asce)0733-9429(2006)132:8(858)

Yang, T., & Shy, S. (2005). Two-way interaction between solid particles and homogeneous air turbulence: Particle settling rate and turbulence modification measurements. *Journal of Fluid Mechanics*, *526*, 171–216. https://doi.org/10.1017/s0022112004002861

References From the Supporting Information

Bonetti, S., Manoli, G., Manes, C., Porporato, A., & Katul, G. (2017). Manning's formula and Strickler's scaling explained by a co-spectral budget model. *Journal of Fluid Mechanics*, *812*, 1189–1212. https://doi.org/10.1017/jfm.2016.863

Li, S., & Katul, G. (2019). Cospectral budget model describes incipient sediment motion in turbulent flows. *Physical Review Fluids*, *4*(9), 093801. https://doi.org/10.1103/physrevfluids.4.093801

Li, S., & Katul, G. (2021). Roughness-induced critical phenomenon analogy for turbulent friction factor explained by a co-spectral budget model. *Physics of Fluids*, *33*(10), 105127. https://doi.org/10.1063/5.0069705